

# The effects of medium on nuclear properties in multifragmentation

J. N. De<sup>1</sup>, S. K. Samaddar<sup>1</sup>, X. Viñas<sup>2</sup>, M. Centelles<sup>2</sup>, I. N. Mishustin<sup>3,4</sup>, and W. Greiner<sup>3</sup>

<sup>1</sup>*Saha Institute of Nuclear Physics,  
1/AF Bidhannagar, Kolkata 700064, India*  
<sup>2</sup>*Departament d'Estructura i Constituents de la Matèria,  
Facultat de Física,  
and Institut de Ciències del Cosmos,  
Universitat de Barcelona,  
Diagonal 645, 08028 Barcelona, Spain*  
<sup>3</sup>*Frankfurt Institute for Advanced Studies,  
J. W. Goethe University,  
D-60438, Frankfurt Am Main, Germany*  
<sup>4</sup>*Kurchatov Institute, Moscow 123182, Russia*

In multifragmentation of hot nuclear matter, properties of fragments embedded in a soup of nucleonic gas and other fragments should be modified as compared with isolated nuclei. Such modifications are studied within a simple model where only nucleons and one kind of heavy nuclei are considered. The interaction between different species is described with a momentum-dependent two-body potential whose parameters are fitted to reproduce properties of cold isolated nuclei. The internal energy of heavy fragments is parametrized according to a liquid-drop model with density and temperature dependent parameters. Calculations are carried out for several subnuclear densities and moderate temperatures, for isospin-symmetric and asymmetric systems. We find that the fragments get stretched due to interactions with the medium and their binding energies decrease with increasing temperature and density of nuclear matter.

PACS numbers: 21.65.-f, 24.10.Pa, 25.70.Pq, 25.70.Mn

Keywords: multifragmentation; nuclear matter; medium effects; nuclear expansion

## I. INTRODUCTION

In energetic nuclear collisions, the participating hot nuclear matter after an initial dynamic stage of compression expands to a subsaturation density and then disassembles into many fragments due to growing instability. Statistical models of different genres [1–6] have generally been successful in explaining the many features associated with the fragment multiplicities, the caloric curve, the density of the fragmenting systems, etc. They also offer a broad hint about the general nature of the phase diagram of nuclear matter [7, 8] at temperature  $T \sim 3$ –8 MeV at subsaturation densities  $\rho \sim 1/20$  to  $1/5$ th of the normal nuclear density  $\rho_0$ . Possible liquid-gas phase transition and associated condensation [9–11] to form nuclear clusters at these temperatures and densities help in a better exploration of many phenomena of astrophysical interest like supernova explosions or explosive nucleosynthesis [12–17].

Analysis of recent laboratory experiments [18, 19] on nuclear multifragmentation seems to indicate that the properties of the nuclides are modified at subnuclear densities ( $\rho \sim \rho_0/3$ ) they are created in corresponding to freeze-out. The symmetry energy, for example, is reported to be progressively reduced [20] with excitation energy, which is attributed to the in-medium modifications of the properties of the hot fragments [21, 22]. A looming uncertainty about whether the measured symmetry energy corresponds to the hot fragments or the

equivocal decision about the medium modifications. The reduction in symmetry energy can have a fair explanation from the thermal and expansion effects of the disassembling system [24]. The surface properties of the hot fragments [25] as well as their bulk energy [26] are also speculated to be modified due to the embedding environment. A quantum statistical approach to the nuclear equation of state taking into account the formation of clusters [27, 28] shows that the properties of these clusters are modified due to the medium in which they are formed. The symmetry energy of low density warm nuclear matter predicted by this model seems to be in good agreement with the experimental data [29]. In a recent experiment [30], it is claimed that the binding energies of very light clusters ( $A \leq 4$ ) produced in multifragmentation progressively tend to zero in the temperature range of  $T \sim 5$  – 10 MeV even at a very low in-medium density  $\sim 0.05 \rho_0$ .

The changes, if any, of the bulk properties of the fragments produced in nuclear disassembly are expected to originate from the effects of the residual interaction of the fragments with the surroundings. The aim of the present article is to study these effects starting from an effective nucleon-nucleon interaction. To keep the physics simple and transparent and yet retaining all the basic essentials, we allow the dilute matter to condense into only one kind of nuclear species surrounded by a hot nucleonic gas and species of the same kind. Then we introduce the interactions between them and look for the minimum of

of the fragments maintaining chemical equilibrium between the fragments and the nucleon gas. The energy and free energy of the nuclei are evaluated in the liquid-drop framework that makes it easier to account for the associated changes in the surface and symmetry energy with the change in the volume of the fragment species.

The organization of the paper is as follows. In Sec. II, the outlines of the theory are given. Results and discussions are contained in Sec. III. The concluding remarks are presented in Sec. IV.

## II. THEORETICAL FORMULATION

As is well known, hot low-density nuclear matter condenses into nuclear fragments of different sizes surrounded by nucleons. We postulate that the nucleons and the fragments interact through a common effective interaction. The bulk properties of the fragments may be modified because of this interaction too. For a qualitative understanding of such system, we take only one kind of fragment species of mass  $A$  and charge  $Z$ . The interaction is chosen to be the modified Seyler-Blanchard (SBM) interaction. Its properties are summarized in Sec. IIA. In Sec. IIB, the method for evaluating the nucleon-fragment and the fragment-fragment interactions is described. In Sec. IIC, we study the observables sensitive to the medium modification of the properties of finite nuclei.

### A. The effective interaction

The SBM interaction is a momentum and density dependent effective interaction of finite range. In the context of the nuclear mass formula, an interaction of this type has been used with great success by Myers and Swiatecki [31]. It also reproduces the rms radii, charge distributions, and giant monopole resonance energies for a host of even-even nuclei ranging from  $^{16}\text{O}$  to very heavy systems [32]. Its form is given by

$$\begin{aligned} v(r, p, \rho) &= C_{l,u} [v_1(r, p) + v_2(r, \rho)], \\ v_1 &= -(1 - \frac{p^2}{b^2})f(\mathbf{r}_1, \mathbf{r}_2), \\ v_2 &= d^2 [\rho(r_1) + \rho(r_2)]^\kappa f(\mathbf{r}_1, \mathbf{r}_2), \end{aligned} \quad (1)$$

with

$$f(\mathbf{r}_1, \mathbf{r}_2) = \frac{e^{-|\mathbf{r}_1 - \mathbf{r}_2|/a}}{|\mathbf{r}_1 - \mathbf{r}_2|/a}. \quad (2)$$

The subscripts  $l$  and  $u$  to the interaction strength  $C$  refer to like-pair (nn or pp) and unlike-pair (np) interactions, respectively. The relative separation of the interacting nucleons is  $\mathbf{r} = \mathbf{r}_1 - \mathbf{r}_2$  and the relative momentum is

TABLE I: The parameters of the effective interaction (in MeV fm units)

$C_l$	$C_u$	$a$	$b$	$d$	$\kappa$
348.5	829.7	0.6251	927.5	0.879	1/6

and  $\kappa$  are listed in Table I. The procedure for determining these parameters are given in detail in Ref. [33]. These parameters are somewhat different from those given in [32]; in the latter, the symmetry coefficient  $a_{sym}$  for infinite nuclear matter at saturation density  $\rho_0$  was chosen to be 34 MeV; in the present calculation, it is taken to be 31 MeV to be more consistent with the recent estimates [34, 35]. The effective mass of the nucleon coming from the momentum dependence of this effective interaction is  $0.62m$  for symmetric nuclear matter, where  $m$  is the nucleon mass. For the interaction, the isoscalar volume incompressibility  $K_\infty$ , symmetry incompressibility  $K_{sym}$  and  $L$ , a measure of the symmetry pressure are 240,  $-101$ , and 59.8 MeV, respectively. It is interesting to note that the symmetry coefficients  $a_{sym}$ ,  $L$ , and  $K_{sym}$  of this interaction are within the range of values suggested by the empirical constraints emerging from recent analysis of different observables [34–40]. With this interaction, for symmetric nuclear matter, the critical temperature is reached at  $T_c = 14.9$  MeV, when the surface energy vanishes.

### B. Nucleon-fragment and fragment-fragment interaction energy

A low-density nucleonic matter of density  $\rho_b$  and asymmetry  $X = (\rho_n^b - \rho_p^b)/\rho_b$  breaks up to a system of free (unbound) neutrons and protons of density  $\rho_n$  and  $\rho_p$  and a collection of mass- $A$  fragments (we call it AN matter), all at temperature  $T$ . The clusterized matter is thermodynamically more favorable than the uniform matter at the same (low) density, asymmetry and temperature [41]. The baryonic density is then given by

$$\rho_b = \rho_N + A\rho_A, \quad (3)$$

where  $\rho_N = \rho_n + \rho_p$  is the free nucleonic density and  $\rho_A$  is the number density of the fragment species. The total thermodynamic potential  $\Omega$  of the system is

$$\Omega = E - TS - \sum_\tau \mu_\tau N_\tau - \mu_A N_A, \quad (4)$$

where  $E, S, \mu_\tau, \mu_A, N_\tau$ , and  $N_A$  are the total energy, entropy, chemical potentials of the free nucleons and the fragments, free nucleon number and the number of the fragments of mass  $A$ , respectively. The isospin index (n,p) is represented by  $\tau$ . Chemical equilibration ensures

$$N_n = N_p = Z, \quad (5)$$

where  $N$  and  $Z$  are the neutron and proton numbers in the fragment. The total internal energy of the AN system is written as

$$E = E_{NN} + E_{AN} + E_{AA}. \quad (6)$$

In Eq. (6),  $E_{AN}$  is the contribution coming from the nucleon-fragment interaction ( $V_{AN}$ ).  $E_{NN}$  measures the kinetic energy of the free nucleons plus the interaction energy amongst themselves.  $E_{AA}$  is the sum total of the kinetic energy of the fragments, interaction energy among them and their binding energies.

Assuming for simplicity that the fragments are sharp-surface liquid drops with a uniform nucleon density  $\rho_l$ , these terms can be explicitly written as,

$$E_{NN} = \sum_{\tau} \left\{ \int d\mathbf{r}_1 d\mathbf{p}_1 \frac{p_1^2}{2m_{\tau}} \tilde{n}_{\tau}(\mathbf{p}_1) + \frac{1}{2} \int d\mathbf{r}_1 d\mathbf{p}_1 d\mathbf{r}_2 d\mathbf{p}_2 \right. \\ \times [v_1(|\mathbf{r}_1 - \mathbf{r}_2|, |\mathbf{p}_1 - \mathbf{p}_2|) + v_2(|\mathbf{r}_1 - \mathbf{r}_2|, 2\rho_N)] \\ \left. \times [C_l \tilde{n}_{\tau}(\mathbf{p}_2) + C_u \tilde{n}_{-\tau}(\mathbf{p}_2)] \tilde{n}_{\tau}(\mathbf{p}_1) \right\}, \quad (7)$$

$$E_{AN} = \frac{1}{2} \sum_{\tau} \left\{ \int d\mathbf{r}_1 d\mathbf{p}_1 d\mathbf{r}_2 d\mathbf{p}_2 \right. \\ \times \tilde{n}_{\tau}(\mathbf{r}_1, \mathbf{p}_1) \tilde{n}_A(\mathbf{r}_2, \mathbf{p}_2) \sum_{\tau'} (C_l \delta_{\tau\tau'} + C_u (1 - \delta_{\tau\tau'})) \\ \times \int_{V_A} d\mathbf{r} \int d\mathbf{p}_{l\tau}^A \tilde{n}_{l\tau'}^A(\mathbf{r}, \mathbf{p}_{l\tau'}^A) [v_1(|\mathbf{r} + \mathbf{R}|, |\mathbf{p}_1 \\ - (\mathbf{p}_{l\tau'}^A + \mathbf{p}_2)|) + v_2(|\mathbf{r} + \mathbf{R}|, \rho_N + \rho_l)] \left. \right\} \quad (8)$$

and,

$$E_{AA} = E_{AA}^0 - N_A B_A(\rho_l, T), \quad (9)$$

where,

$$E_{AA}^0 = \int d\mathbf{r} d\mathbf{p} \frac{p^2}{2m_A} \tilde{n}_A(\mathbf{r}, \mathbf{p}) + \frac{1}{2} \int d\mathbf{r}_1 d\mathbf{p}_1 d\mathbf{r}_2 d\mathbf{p}_2 \\ \times \tilde{n}_A(\mathbf{r}_1, \mathbf{p}_1) \tilde{n}_A(\mathbf{r}_2, \mathbf{p}_2) \int_{V_A} d\mathbf{r} d\mathbf{r}' \\ \times \sum_{\tau, \tau'} (C_l \delta_{\tau\tau'} + C_u (1 - \delta_{\tau\tau'})) \int d\mathbf{p}_{l\tau}^A d\mathbf{p}_{l\tau'}^A \\ \times \tilde{n}_{l\tau}^A(\mathbf{r}, \mathbf{p}_{l\tau}^A) \tilde{n}_{l\tau'}^A(\mathbf{r}', \mathbf{p}_{l\tau'}^A) [v_1(|\mathbf{R} + \mathbf{r} - \mathbf{r}'|, |(\mathbf{p}_1 \\ + \mathbf{p}_{l\tau}^A) - (\mathbf{p}_2 + \mathbf{p}_{l\tau'}^A)|) \\ + v_2(|\mathbf{R} + \mathbf{r} - \mathbf{r}'|, 2\rho_l)]. \quad (10)$$

In Eq. (8),  $\mathbf{R} = \mathbf{r}_2 - \mathbf{r}_1$  is the distance between the nucleon and the center of the nucleus (see Fig. 1). In Eq. (10),  $\mathbf{R}$  is the distance between the two fragment centers (see Fig. 2). The various space coordinates occurring in Eqs. (8) and (10) are explained in Figs. 1 and 2.

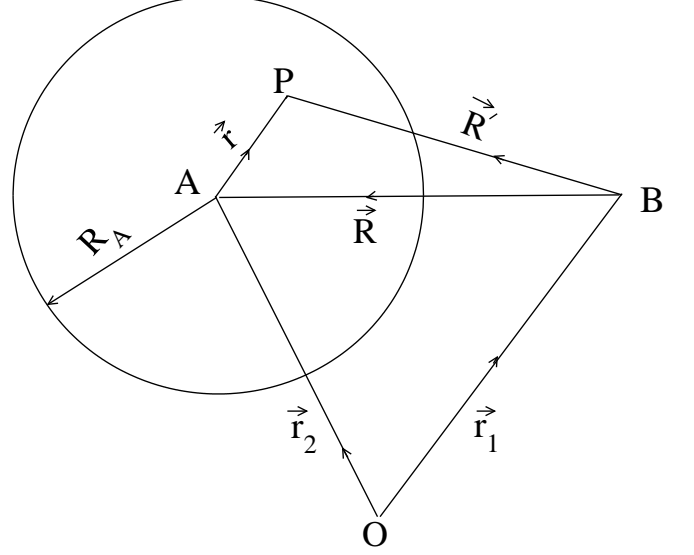


FIG. 1: Space coordinates shown for nucleon (located at  $B$ ) and fragment (with center at  $A$ ) configuration. The origin of the coordinate system is at  $O$  and  $P$  is any arbitrary point within the fragment.

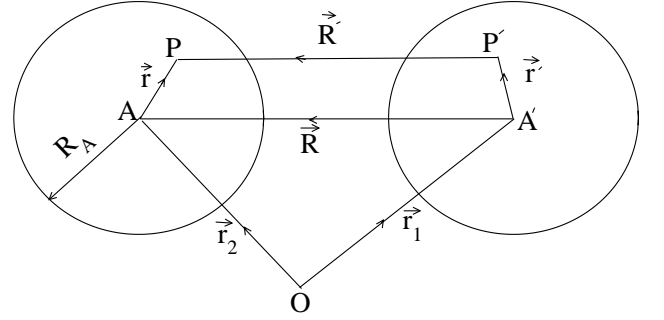


FIG. 2: Space coordinates shown for fragment-fragment configuration with  $O$  as the origin of the coordinate system.  $P$  and  $P'$  are arbitrary points within the fragments with  $A$  and  $A'$  as their centers.

respectively. In evaluating the coordinate-space integrals in Eqs. (7), (8) and (10), we have assumed, as in the calculation of the equation of state of dilute nuclear matter [42, 43] that the free nucleons do not penetrate the sharp surface nuclei and also that the fragments do not interpenetrate so that the identity of the free nucleons and the fragments is never altered. This 'no-overlap' approximation is tantamount to use of the 'excluded-volume' correction employed earlier [2] where the 'free' volume available to fragments is reduced compared to the total volume  $V$  by at least the internal volume of the nucleons and the fragments.

In the above equations,  $m_{\tau}$  and  $m_A$  are the masses of the nucleons and the fragments, and  $B_A(\rho_l, T)$  is the binding energy of the produced fragments at temperature  $T$  with initial nucleon density  $\rho_l$ . Here,  $\tilde{n}_{\tau} = \frac{2}{h^3} \int d\mathbf{p} \tilde{n}_{\tau}(\mathbf{p})$

$\tilde{n}_A = \frac{g_A}{h^3} n_A$ ;  $n_\tau$  and  $n_A$  are the occupation probabilities for the free nucleons and the fragments and  $g_A$  is the degeneracy of the fragments taken to be 1 or 2 depending on whether they are bosons or fermions. Since the system is infinite, the occupation functions  $\tilde{n}_\tau$  are independent of space coordinates. Similar is the case for  $\tilde{n}_A$ . In the equations above, space dependence has, however, been retained to correlate with Figs. 1 and 2. Since the fragments are also taken to be uniform drops,  $\tilde{n}_{l\tau}^A (= \frac{2}{h^3} n_{l\tau}^A)$ , the distribution function of the constituent nucleons inside the fragments is also independent of the space coordinates. The explicit functional dependence of the distribution functions on the space coordinates is henceforth omitted from the equations where the distribution functions may enter. The momenta of these nucleons inside the fragment is designated by  $\mathbf{p}_{l\tau}^A$ . The notation  $\int_{V_A}$  refers to the configuration integral over the volume  $V_A$  of the fragment. All other integrals are over the entire configuration or momentum space unless otherwise specified. The distribution functions yield the densities as,

$$\frac{2}{h^3} \int n_\tau(\mathbf{p}) d\mathbf{p} = N_\tau/V = \rho_\tau, \quad (11)$$

$$\frac{2}{h^3} \int n_A(\mathbf{p}) d\mathbf{p} = N_A/V = \rho_A, \quad (12)$$

$$\frac{2}{h^3} \int n_{l\tau}^A(\mathbf{p}) d\mathbf{p} = A_\tau/V_A = \rho_{l\tau}, \quad (13)$$

where  $V$  is the volume of the AN matter,  $A_\tau$  is the neutron number  $N$  or proton number  $Z$  in the fragment,  $\rho_N = \sum_\tau \rho_\tau$ ,  $\rho_l = \sum_\tau \rho_{l\tau}$  and  $V_A = \frac{4\pi}{3} R_A^3$ . In Eq. (13),  $\rho_{l\tau}$  refers to the neutron or proton number density in the fragment;  $R_A$  is its sharp-surface radius.

The total entropy of the AN system is

$$S = \sum_\tau S_\tau + S_A^{tr} + S_A^{int}, \quad (14)$$

where in the Landau quasiparticle approximation, the contribution  $\sum_\tau S_\tau$  of the free nucleons is taken as

$$\begin{aligned} \sum_\tau S_\tau = & -\frac{2}{h^3} \sum_\tau \int d\mathbf{r} d\mathbf{p} \left[ n_\tau(\mathbf{p}) \ln n_\tau(\mathbf{p}) \right. \\ & \left. + (1 - n_\tau(\mathbf{p})) \ln(1 - n_\tau(\mathbf{p})) \right]. \end{aligned} \quad (15)$$

$S_A^{tr}$  is the entropy from the center-of-mass motion of the fragments, and  $S_A^{int}$  is their internal entropy.  $S_A^{tr}$  is evaluated as,

$$\begin{aligned} S_A^{tr} = & -\frac{g_A}{h^3} \int d\mathbf{r} d\mathbf{p} [n_A(\mathbf{p}) \ln n_A(\mathbf{p}) \\ & \pm (1 \mp n_A(\mathbf{p})) \ln(1 \mp n_A(\mathbf{p}))]. \end{aligned} \quad (16)$$

In the above equation, the upper and lower signs correspond to a fermionic and bosonic fragment, respectively. The contribution  $S_A^{int}$  from internal degrees of freedom

the thermodynamic potential can be absorbed along with the binding energy term of Eq. (9) in the free energy of the fragments  $F_A(\rho_l, T) = (-B_A(\rho_l, T) - TS_A^{int})$  when the thermodynamic potential takes the form,

$$\begin{aligned} \Omega = & E_{NN} + E_{AN} + E_{AA}^0 - T \left( \sum_\tau S_\tau + S_A^{tr} \right) \\ & - \sum_\tau \mu_\tau N_\tau - \mu_A N_A + N_A F_A(\rho_l, T) \end{aligned} \quad (17)$$

Minimization of  $\Omega$  with respect to  $n_\tau$  and  $n_A$ , remembering that  $\delta n_\tau(\mathbf{p})$  and  $\delta n_A(\mathbf{p})$  are separately arbitrary over the whole phase space, after some algebraic manipulations, yields for the distribution functions with the following structures,

$$n_\tau(\mathbf{p}) = \left[ \exp \left( \frac{p^2}{2m_\tau^* T} - \eta_\tau \right) + 1 \right]^{-1}, \quad (18)$$

$$n_A(\mathbf{p}) = \left[ \exp \left( \frac{p^2}{2m_A^* T} - \eta_A \right) \pm 1 \right]^{-1}. \quad (19)$$

In Eqs. (18) and (19),  $\eta_\tau = (\mu_\tau - V_\tau^0 - V_\tau^2)/T$  and  $\eta_A = (\mu_A - F_A - V_A^0)/T$  are the fugacities pertaining to the free nucleons and fragments, respectively and  $m_\tau^*$  and  $m_A^*$  are the effective masses of the nucleons and the fragments in the medium, the masses getting renormalized owing to the momentum dependence of the force. The nucleonic rearrangement potential  $V_\tau^2$  originates from the density dependence of the interaction. The effective nucleon and fragment masses are given by

$$m_\tau^* = \left[ \frac{1}{m_\tau} + 2V_\tau^1 \right]^{-1}, \quad (20)$$

and

$$m_A^* = \left[ \frac{1}{m_A} + 2V_A^1 \right]^{-1}, \quad (21)$$

where  $p^2 V_\tau^1$  and  $p^2 V_A^1$  are the momentum dependent contributions to the single-particle potentials  $V_\tau$  and  $V_A$ :

$$V_\tau(p) = V_\tau^0 + p^2 V_\tau^1, \quad (22)$$

$$V_A(p) = V_A^0 + p^2 V_A^1. \quad (23)$$

Expressions for the momentum independent components  $V_\tau^0$  and  $V_A^0$ , along with those for  $V_\tau^1$ ,  $V_\tau^2$  and  $V_A^1$  are given in the Appendix.

### C. Energy and free energy of the system

We take recourse to liquid-drop model for the evaluation of the total energy  $E$  (Eq. (9)) of the fragments of

mass  $A$ , charge  $Z$  and neutron number  $N$  at a constant density  $\rho$  and temperature  $T$ . The energy  $E_A(\rho, T)$  ( $= -B_A(\rho, T)$ ) is given by

$$E_A(\rho, T) = a_v(\rho, T)A + a_s(\rho, T)4\pi R_A^2 A^{2/3} + a_{sym}(\rho, T)\frac{(N-Z)^2}{A} + \frac{3}{5}Z^2 e^2 \left( \frac{1}{R_A} - \frac{1}{R_{WS}} \right). \quad (24)$$

The term  $a_v$  is the volume energy term for symmetric nuclear matter. Alongwith  $a_v$ , the surface energy coefficient  $a_s$  and the symmetry energy coefficient  $a_{sym}$  are all density and temperature dependent. The last term in Eq. (24) is the the Coulomb term. One may note that the Coulomb energy is different from that for an isolated nucleus. As the fragment is embedded in clusterized matter, its Coulomb energy gets 'dressed'. It is calculated in the Wigner-Seitz approximation [2]. Here  $R_{WS}$  is the radius of the spherical Wigner-Seitz cell, given as  $R_{WS} = (\frac{4}{3}\pi\rho_A)^{-1/3}$ . The Coulomb energy has no explicit temperature dependence. The radius  $R_A$  of the liquid drop is given by  $R_A = A^{1/3}/[\frac{4}{3}\pi\rho(T)]^{1/3}$ . In a similar vein to Eq. (24), the free energy of the nucleus is taken as

$$F_A(\rho, T) = f_v(\rho, T)A + f_s(\rho, T)4\pi R_A^2 A^{2/3} + f_{sym}(\rho, T)\frac{(N-Z)^2}{A} + \frac{3}{5}Z^2 e^2 \left( \frac{1}{R_A} - \frac{1}{R_{WS}} \right). \quad (25)$$

The volume terms  $a_v$  and  $f_v$  are calculated for symmetric nuclear matter at density  $\rho$  and at temperature  $T$  employing the SBM interaction. The density and temperature dependence of the surface free energy coefficient is assumed to be factorized [44] and is taken as

$$f_s(\rho, T) = a_s(\rho_0, T=0)\mathcal{U}(\rho)\mathcal{Y}(T), \quad (26)$$

where  $a_s(\rho_0, T=0)$  is the surface energy coefficient at nuclear matter saturation density  $\rho_0$  at  $T=0$ . The expressions for  $\mathcal{U}(\rho)$  and  $\mathcal{Y}(T)$  are taken from Refs. [45] and [2], respectively. They are given as

$$\mathcal{U}(\rho) = 1 - \frac{k_\rho}{2} \left( \frac{\rho - \rho_0}{\rho_0} \right)^2, \quad (27)$$

and

$$\mathcal{Y}(T) = \left( \frac{T_c^2 - T^2}{T_c^2 + T^2} \right)^{5/4}. \quad (28)$$

$T_c$  is the critical temperature for nuclear matter calculated to be 14.9 MeV with the SBM interaction. The value of  $a_s(\rho_0, T=0)$  and  $k_\rho$  are taken to be 1.15 MeVfm<sup>-2</sup> and 5.0, respectively. The surface entropy per unit area  $\mathcal{S}_{surf}$  is obtained from  $f_s$  as

$$\mathcal{S}_{surf} = - \left. \frac{\partial f_s}{\partial T} \right|_\rho, \quad (29)$$

which yields

$$a_s(\rho, T) = f_s(\rho, T) + T\mathcal{S}_{surf} = a_s(\rho_0, 0) \left[ \mathcal{Y}(T) + 5 \left( \frac{T_c^2 - T^2}{T_c^2 + T^2} \right)^{1/4} \times \frac{T_c^2 T^2}{(T_c^2 + T^2)^2} \right] \mathcal{U}(\rho). \quad (30)$$

The symmetry coefficient  $a_{sym}$  is dependent on the nuclear mass. It is taken as [35]

$$a_{sym}(\rho = \rho_0, T=0) = \frac{\alpha}{1 + \frac{\alpha}{\beta} A^{-1/3}}, \quad (31)$$

where  $\alpha$  is the symmetry coefficient of cold symmetric nuclear matter taken as 31.0 MeV and  $\frac{\alpha}{\beta} = 2.4$ . For infinite matter, it is generally seen that  $a_{sym}$  decreases with temperature whereas  $f_{sym}$  shows the opposite temperature dependence [46]. A nearly similar trend has been observed for finite nuclei [47]; here  $f_{sym}$  increases with temperature (though in some cases, an occasional decrease is seen at low  $T$ ). The density dependence of the symmetry energy of nuclear matter calculated with the SBM interaction is seen to be given by  $\sim (\rho/\rho_0)^\gamma$  with  $\gamma \sim 0.69$  [24], in consonance with the reported experimental behavior [20]. With this in mind, we write the symmetry free energy coefficient in a factorized form as

$$f_{sym}(\rho, T) = a_{sym}(\rho, T=0)g(T), \quad (32)$$

where

$$a_{sym}(\rho, T=0) = a_{sym}(\rho_0, T=0)(\rho/\rho_0)^\gamma. \quad (33)$$

For  $g(T)$ , we assume a polynomial in  $T$  of the form,

$$g(T) = (1 + \nu_1 T + \nu_2 T^2 + \nu_4 T^4). \quad (34)$$

Then,

$$\mathcal{S}_{sym} = - \left. \frac{\partial f_{sym}}{\partial T} \right|_\rho, \quad (35)$$

and therefore

$$a_{sym}(\rho, T) = f_{sym}(\rho, T) - T \left. \frac{\partial f_{sym}(\rho, T)}{\partial T} \right|_\rho \quad (36)$$

$$= a_{sym}(\rho, T=0)[1 - \nu_2 T^2 - 3\nu_4 T^4]. \quad (37)$$

In a schematic model [47], the observed  $T$ -dependence of  $a_{sym}$  and  $f_{sym}$  has been seen to be moderately explained with values of  $\nu_1, \nu_2$ , and  $\nu_4$  as  $-0.00848, 0.00201$  and  $0.0000147$ , respectively, the dimensions of these quantities being in relevant inverse powers of MeV.

The internal entropy  $S_A^{int}$  of the fragments has contributions from the volume, surface, and the asymmetry. The latter two contributions have already been taken into

the fragments are taken to have uniform density  $\rho$ , the volume entropy is calculated using the expression given in Eq. (15) for symmetric nuclear matter at temperature  $T$  and at a density  $\rho$ .

Combining the terms given by Eqs. (7)-(10), the total energy of the (n,p,A) system can then be written as,

$$E = V \left[ \left\{ \sum_{\tau} \rho_{\tau} T J_{3/2}(\eta_{\tau}) / J_{1/2}(\eta_{\tau}) \right. \right. \\ \times (1 - m_{\tau}^* V_{\tau}^*) + \frac{1}{2} \rho_{\tau} V_{\tau}^0 \left. \right\} + \rho_A T C_A \\ \times (1 - m_A^* V_A^1) + \frac{1}{2} \rho_A V_A^0 - \rho_A B_A(\rho_l, T) \left. \right]. \quad (38)$$

We may remind here that  $\rho_{\tau}$  corresponds to the free nucleonic density after condensation. The total entropy of the free nucleonic matter is, from Eq. (15),

$$\sum_{\tau} S_{\tau} = V \sum_{\tau} \rho_{\tau} \left[ \frac{5}{3} J_{3/2}(\eta_{\tau}) / J_{1/2}(\eta_{\tau}) - \eta_{\tau} \right]. \quad (39)$$

Similarly, the translational entropy from the fragments is,

$$S_A^{tr} = N_A \left[ \frac{5}{3} C_A - \eta_A \right], \quad (40)$$

where  $C_A$  is given by,

$$C_A = J_{3/2}(\eta_A) / J_{1/2}(\eta_A), \quad (41)$$

or

$$C_A = B_{3/2}(\eta_A) / B_{1/2}(\eta_A), \quad (42)$$

depending on whether the fragments are fermionic or bosonic. In the above equations, the quantities  $J_k$  and  $B_k$  are the Fermi and Bose integrals; their definitions are given in Eq. (A.4) in the Appendix A. As the fragment densities are usually very low,  $C_A \sim 3/2$ . Since the internal entropy  $S_A^{int}$  of the fragments is now known as explained earlier, the free energy  $\mathcal{F}$  of the total AN matter can be calculated.

### III. RESULTS AND DISCUSSIONS

In this paper, our primary aim is to investigate the changes in the properties of nuclei embedded in a hot medium of nucleons and other fragments produced in nuclear multifragmentation. To simplify the problem yet retaining the main physics essence, we assume that after nuclear disassembly, the system contains a collection of only one kind of fragments of mass  $A$  and charge  $Z$  in thermodynamic equilibrium, with a hot soup of neutrons and protons. To begin with, we take a baryon matter

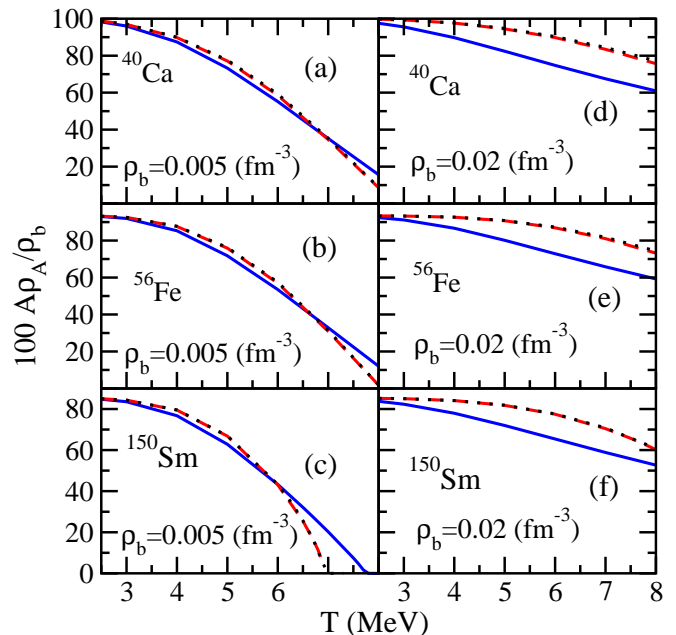


FIG. 3: (Color online) The percentage of nucleons contained in the fragments at a given baryon density  $\rho_b$  at  $X = 0.0$  shown as a function of temperature after fragmentation. The left panels correspond to  $\rho_b = 0.005 \text{ fm}^{-3}$ , the right panels to  $\rho_b = 0.02 \text{ fm}^{-3}$ . The fragment specimens chosen are  $^{40}\text{Ca}$ ,  $^{56}\text{Fe}$  and  $^{150}\text{Sm}$ , respectively. The blue full line corresponds to the case (1,1,1), i.e., the calculation where all three interactions NN, AN, and AA are included. The red dashed line refers to the case (1,0,1) where the AN contribution is neglected, whereas the black dotted line corresponds to the (1,0,0) calculation without both the AN and AA contributions. For details, see text.

asymmetry  $X$ . The binding energies and the free energies of the nuclear fragments that enter into the calculation have been modeled in the context of the liquid drop mass formula. For the effective interaction, the momentum and density dependent SBM force as scripted in Eqs. (1) and (2) has been chosen. Assumptions are made that the free nucleons do not penetrate the sharp-surface nuclei and that the fragments do not overlap.

The three unknowns in the calculation are the free nucleon densities  $\rho_n, \rho_p$  and the fragment densities  $\rho_A$  in the matter. The three constraints are the conservation of the total baryon number, the total isospin and the condition of chemical equilibrium between the nucleon gas and the fragments. For a given set of  $\rho_b, T$  and  $X$ , the calculations start with a chosen value of the density  $\rho_l$  of the constituent nucleons in the nuclear fragments at temperature  $T$  and an input guess density of  $\rho_A$ . The energies and the free energies of the fragments are then known from Eqs (24) and (25). Exploiting the constraints, the final densities  $\rho_A, \rho_n$  and  $\rho_p$  are determined iteratively. The total free energy  $\mathcal{F}$  of the given AN matter (see Eqs (6) and (14)) is then calculated as outlined earlier. Changing the input values of  $\rho_b, T$  and  $X$ , the calculation

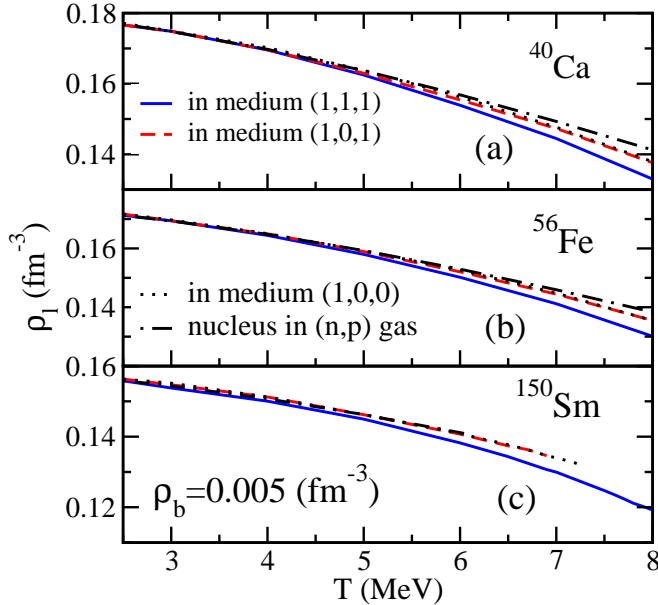


FIG. 4: (Color online) The nucleon number density in the fragments shown as a function of temperature, for baryon density  $\rho_b = 0.005 \text{ fm}^{-3}$  at  $X = 0.0$ . The blue full line, red dashed line and the black dotted line convey the same meaning as in Fig. 3. The dash-dot (black) lines refer to the nuclear density when the nuclei ( $^{40}\text{Ca}$ ,  $^{56}\text{Fe}$  or  $^{150}\text{Sm}$ ) are in phase equilibrium with their own vapor.

determines  $\rho_l$  at a given baryonic density  $\rho_b$  with asymmetry  $X$  at temperature  $T$ , which then, in the liquid drop framework, determines all the properties under investigation of the produced fragments.

The calculations have been done in the temperature range 2.5–8 MeV for symmetric and asymmetric nuclear matter. Initially a symmetric matter ( $X = 0.0$ ) of low baryon density  $\rho_b = 0.005 \text{ fm}^{-3}$  is chosen, and the calculations are then repeated at a higher baryon density  $\rho_b = 0.02 \text{ fm}^{-3}$ . This helps to see how a denser medium accentuates changes in the nuclear properties. Three representative fragments are selected, namely,  $^{40}\text{Ca}$ ,  $^{56}\text{Fe}$  and a heavier one  $^{150}\text{Sm}$ . In Fig. 3, the percentage of nucleons in the fragments produced ( $A\rho_A/\rho_b \times 100$ ) is shown as a function of temperature for the three fragment species. The left panels correspond to  $\rho_b = 0.005 \text{ fm}^{-3}$ , the right panels refer to the higher baryon density  $\rho_b = 0.02 \text{ fm}^{-3}$ . The blue full line is obtained from calculations with inclusion of all three interaction contributions, namely, (NN), (AN), and (AA) [see Eqs. (7)–(10)]. We refer to these calculations as (1,1,1). The dashed red line corresponds to calculations without the (AN) contribution and the dotted black line is the one obtained when both (AN) and (AA) contributions are excluded. The latter two calculations are referred to (1,0,1) and (1,0,0), respectively. At low temperatures, most of the nucleons are contained in the fragments and the free nucleons are rare. This is expected, vapor tends to condense to drops at low temper-

probability decreases. Fragment formation also depends on the total baryon density  $\rho_b$ ; at the higher  $\rho_b$ , fragment formation probability is higher. As the system heats up, this probability goes down.

Examination of the figure reveals few further features. The nucleus-nucleus interaction (AA) does not have a very significant role (as seen from the almost overlapping of the red dashed (1,0,1) and black dotted (1,0,0) lines), the nucleon-nucleus interaction (AN) is important, the importance grows with increasing baryon density  $\rho_b$ . Normally, it is seen that the (1,0,1) or (1,0,0) calculations favor the production of fragments compared to a full (1,1,1) calculation. These results allow us to conclude that heavy nuclei embedded in the medium are affected mostly by the nucleons (and perhaps light clusters) surrounding them. This means that the description of the multicomponent nuclear system can be simplified by subdividing it into non-interacting cells containing one heavy nucleus and a proportional amount of the medium. This Wigner-Seitz approximation is widely used for studying inhomogeneous phases of nuclear matter [48–50].

In Fig. 4, the progressive changes in the internal nucleonic density in the three nuclei produced from disassembly of symmetric nuclear matter of density  $\rho_b = 0.005 \text{ fm}^{-3}$  are displayed as a function of temperature in the three panels. The blue (full line), red (dashed) and the black (dotted) lines have the same meaning as stated earlier. The dash-dot black line refers to calculations for isolated hot nuclei ( $^{40}\text{Ca}$ ,  $^{56}\text{Fe}$  or  $^{150}\text{Sm}$ ) in phase equilibrium with their own vapor (n-p gas). In that case, the phase-equilibrium conditions [51] determine the density and asymmetry of the embedding nucleonic gas along with the internal density of the dipped nucleus. The dot-dash black line is drawn so as to serve as a reference against which the other ones can be compared. In this case thermodynamic equilibrium ensures that the temperatures of the nucleus and the surrounding (n,p) gas are the same, the pressure exerted by the nucleus balances that of the gas and that the chemical potentials of the neutrons and protons of the nucleus are the same as those of the free neutrons and protons in the gas, respectively. Discussion on this part of physics is left out here, it is given in detail in Ref. [51, 52]. The densities of the embedding n-p gas in clusterized matter and in the case of isolated hot nucleus are somewhat different. In both cases the density of the surrounding n-p gas is low at low temperatures and increases with increase in temperature. The asymmetry of this gas is also different in both cases. As an illustrative example, these properties of the embedding nucleonic gas are displayed in Fig. 5. The asymmetry of the disassembling system is  $X = 0.2$  and the fragment concerned is  $^{150}\text{Sm}$ . The asymmetry of the gas has a very insignificant role to play on the properties of the fragments as will be shown later.

From Fig. 4, it transpires as expected, the fragment nuclei in equilibrium in an embedding medium expand with temperature in all four calculations displayed in this fig-

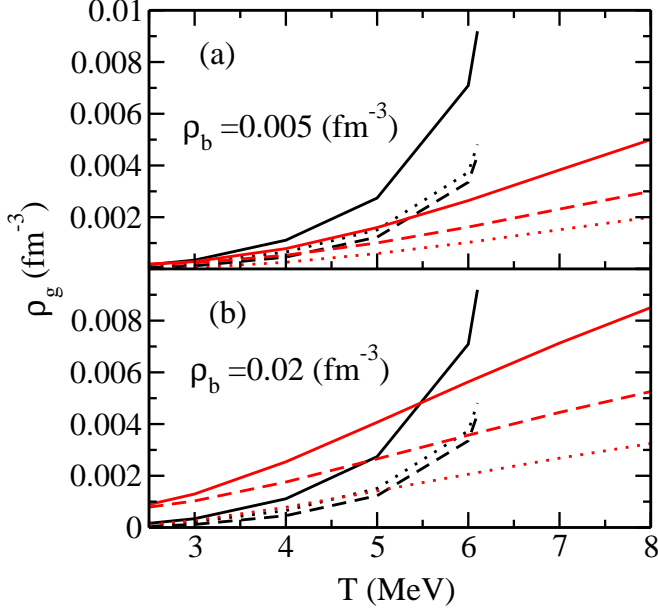


FIG. 5: (Color online) The embedding nucleon gas density plotted as a function of temperature in AN matter where A is  $^{150}\text{Sm}$ . The panels (a) and (b) correspond to  $\rho_b = 0.005 \text{ fm}^{-3}$  and  $0.02 \text{ fm}^{-3}$ , respectively. The red dotted, dashed and full lines refer to proton and neutron densities and their sum in the calculation for disassembled matter at asymmetry  $X = 0.2$ . The black dotted, dashed and full lines correspond to proton and neutron densities and their sum in the phase-equilibrium calculation for  $^{150}\text{Sm}$ .

nuclei like  $^{40}\text{Ca}$  or  $^{56}\text{Fe}$  bloat up in volume by  $\sim 17$ – $19\%$  from their ground state equilibrium values when the temperature is raised to  $\sim 7$ – $8 \text{ MeV}$ . In the full (1,1,1) fragmentation calculation for nuclear matter at  $\rho_b = 0.005 \text{ fm}^{-3}$  they do so by  $\sim 25\%$ . As is seen from the figure, incorporation of the nucleon-fragment (AN) interaction plays a significant role in the expansion of the fragments; also it is seen, as stated earlier, that the fragment-fragment interaction (AA) has little effect. In panel (c) of Fig. 4, it is noticed that the black dash-dot line does not extend beyond  $6.1 \text{ MeV}$ . This is the limiting temperature as obtained for  $^{150}\text{Sm}$  in the phase equilibrium calculation. Solutions for calculations without incorporation of both AN and AA (1,0,0) interactions and for calculations without AN interactions (1,0,1) could not be obtained for this nucleus beyond  $7.2$  and  $6.9 \text{ MeV}$ , respectively. The so-found absence of solutions possibly points to the nuclear instability beyond these temperatures in these calculations. When the baryon density  $\rho_b$  is increased, the nuclear soup of fragments and nucleons becomes denser. In this denser environment, a further expansion of the fragments, by another  $\sim 4\%$  could be noticed. This is displayed in Fig. 6 where  $\rho_b = 0.02 \text{ fm}^{-3}$ . The (1,0,1) and (1,0,0) calculations for  $^{150}\text{Sm}$  could now be extended to  $8.0 \text{ MeV}$ .

As the internal density of the nuclei change progres-

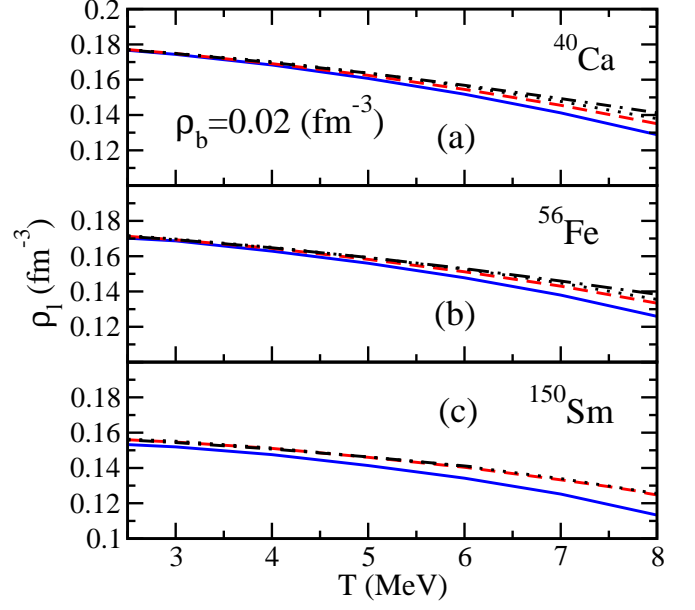


FIG. 6: (Color online) Same as in Fig. 4 when  $\rho_b = 0.02 \text{ fm}^{-3}$ .

reference calculation as mentioned earlier, it is expected that there should be a corresponding change in the binding energies and free energies of the nuclei embedded in medium. We display those quantities for  $^{40}\text{Ca}$  in Fig. 7. The left panels (a) and (b) show the results for the lower baryon density  $\rho_b = 0.005 \text{ fm}^{-3}$ , the right panels (c) and (d) do so for  $\rho_b = 0.02 \text{ fm}^{-3}$ , both at  $X = 0.0$ . The upper panels display the binding energy, the lower panels the free energy. The (1,0,0) calculations being nearly indistinguishable from the (1,0,1) calculations are not shown here. The results for the binding energies from the (1,1,1) and (1,0,1) calculations at the lower baryon density are nearly indistinguishable from each other, at the higher baryon density ( $\rho_b = 0.02 \text{ fm}^{-3}$ ) only little changes are observed at the high temperatures. Compared to the reference calculation (dash-dot black line representing phase equilibrium in a n-p gas), there is a gain in the binding energy. This comes mostly from the decrease of the Coulomb energy because of the presence of other fragments (see Eq. 24). At higher baryon density, the fragment density is comparatively higher which explains the larger gap in binding energy with reference to the phase equilibrium calculation. For a given baryon density the reduction in the density of the fragments with temperature reduces the gap. Similar arguments follow for the lower free energy of the embedded fragments as compared to that from the reference calculation. Not much of a difference is seen for the heavier nucleus  $^{150}\text{Sm}$  as displayed in Fig. 8.

In order to see the importance of asymmetry on the fragment observables, the calculations have been repeated for asymmetric nuclear matter with  $X = 0.2$ . In Fig. 9, comparison of the percentage of nucleons con-

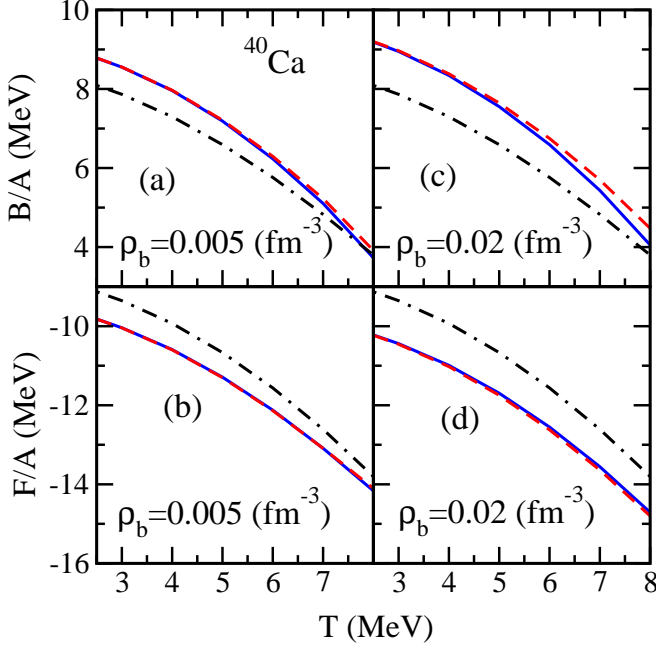


FIG. 7: (Color online) The binding energy and free energy of  $^{40}\text{Ca}$ , produced in fragmentation of symmetric nuclear matter. The left panels refer to  $\rho_b = 0.005 \text{ fm}^{-3}$ , the right panels correspond to  $\rho_b = 0.02 \text{ fm}^{-3}$ . The full (blue), dashed (red) and the dash-dot (black) lines have the same meaning as in Fig. 4.

asymmetric nuclear matter at the two baryon densities we have considered for the three fragment species. We display only the full calculations (1,1,1). The blue full lines correspond to  $X = 0.0$ , the blue dotted lines refer to  $X = 0.2$ .  $^{40}\text{Ca}$  and  $^{56}\text{Fe}$  being symmetric and nearly symmetric nuclei, respectively have comparatively larger population in symmetric nuclear matter. For the more asymmetric  $^{150}\text{Sm}$  nucleus, population is larger in the asymmetric matter. The difference between the two calculations at the two asymmetries is more pronounced at lower temperatures gradually narrowing down as the temperature is raised. The internal nucleon density of the fragments and their binding energies, however, show no significant change when the isospin asymmetry of the matter changes. This is displayed in Fig. 10 and Fig. 11, respectively for the three nuclear fragments at the two baryon densities; the blue full and dotted lines nearly overlap each other over the whole temperature range we work in.

#### IV. CONCLUDING REMARKS

Analysis of nuclear multifragmentation data showed that for the results calculated in thermodynamic models to conform to the experimentally observed ones, the established nuclear parameters taken as inputs in these calculations should be modified [21, 22, 25, 26]. Such

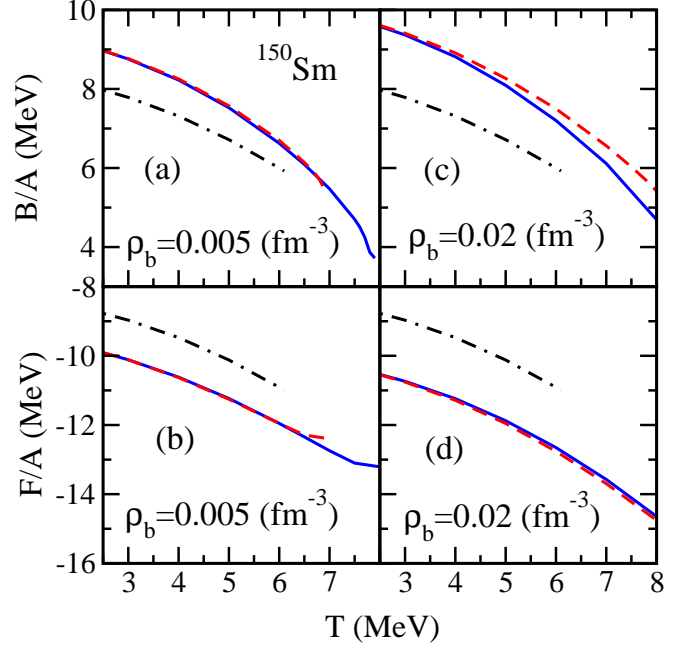


FIG. 8: (Color online) Same as in Fig. 7 for  $^{150}\text{Sm}$ .

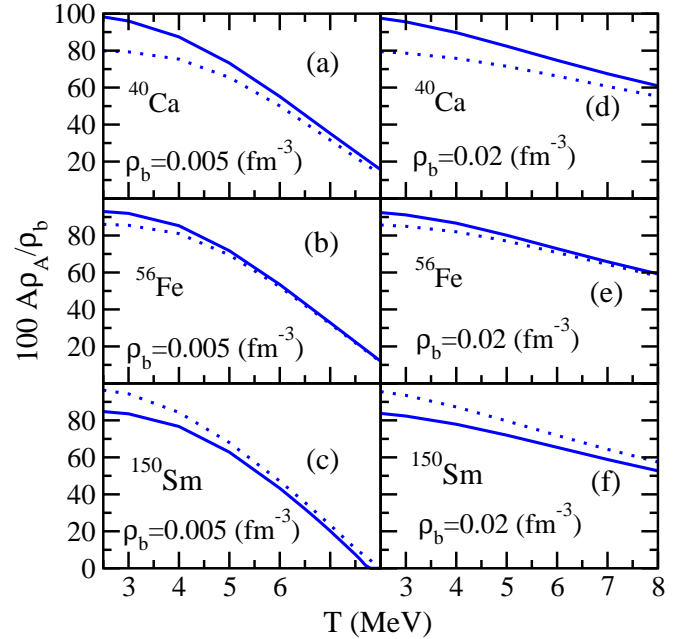


FIG. 9: (Color online) Comparison of fragment population in symmetric and asymmetric nuclear matter for the case (1,1,1) calculated for two baryon densities. The full and dotted lines correspond to  $X = 0.0$  and  $X = 0.2$ , respectively.

a fact points out that the properties of the fragments produced in nuclear disassembly might have got modified because of the interaction of the fragments with the embedding environment they are created in. The calculations presented in this paper throw light in a quantitative manner on the isospin asymmetry of the fragments.

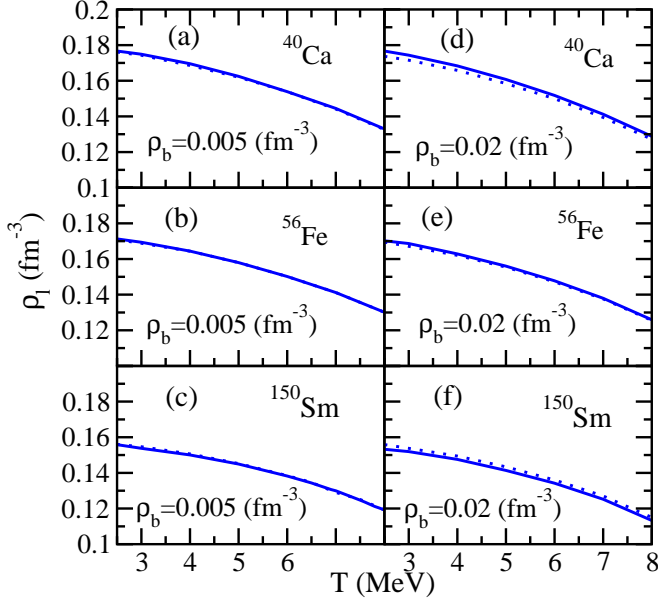


FIG. 10: (Color online) Comparison of the internal nucleon densities of the fragments produced in symmetric and asymmetric ( $X = 0.2$ ) nuclear matter calculated for two baryon densities. The full and dotted lines have the same meaning as in Fig. 9.

be. For simplicity, the fragmented system was assumed to contain a collection of only one kind of nuclear species in addition to neutrons and protons. For comparison, a benchmark calculation of the hot fragments in phase-equilibrium with its own vapor was also done. In both cases, it was seen that the fragments expand with temperature as expected, but compared to the results from the phase-equilibrium (benchmark) calculation, the embedding medium in multifragmentation produced larger changes in the fragment properties. The fragments get comparably more stretched; the volume energy, surface properties or the symmetry properties of the fragments undergo the consequential changes.

Questions may arise on the justification of the choice of only one kind of species in the calculations. Close examination of the results shows that in the medium, the interaction of the nucleons with the fragments plays the dominant role in bringing forth the modification in the fragment properties. The fragment-fragment interaction has a very nominal role. The selection of the multispecies in the medium may not thus possibly alter the results much.

Experiments with intermediate energy heavy ion beams in the last few decades have indicated [53] that nuclei can sustain only temperatures that are much lower than the critical temperature ( $\sim 16$  MeV) for symmetric nuclear matter. The origin of such a limiting temperature is usually traced to an interplay between the Coulomb instability and the corrections due to the finite size of the nuclear drops. Phase-equilibrium calculations for hot iso-

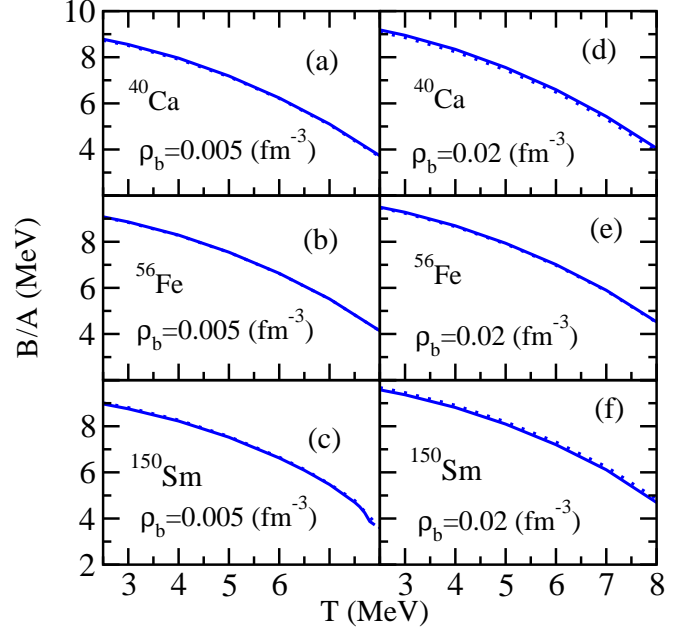


FIG. 11: (Color online) Comparison of the binding energies of the fragments produced in symmetric and asymmetric ( $X = 0.2$ ) nuclear matter calculated for two baryon densities. The full and dotted lines have the same meaning as in Fig. 9.

temperatures  $\sim 5-7$  MeV for heavier nuclei [51, 52, 54]. In the calculations presented in this paper, it is seen that for nuclei dripped in a nuclear soup, the interaction with the surrounding medium might overcome the said instability to a certain extent and extend somewhat the limit in temperature the nuclei may hold. This might be of significant relevance in the context of nuclear astrophysics and needs further exploration.

### Acknowledgments

J.N.D and S.K.S acknowledge the support of DST, Government of India. M.C. and X.V. acknowledge the support of the Consolider Ingenio 2010 Programme CPAN CSD2007-00042, of the grants FIS2011-24154 from MICINN and FEDER, and of grant 2009SGR-1289 from Generalitat de Catalunya. I.N.M acknowledges support from grant NSH-215.2012.2, Russia.

### Appendix A

From Eqs. (11) and (18), the density of the free nucleons  $\rho_\tau$  is found to be

$$\rho_\tau = \frac{4\pi}{3} (2m^*T)^{3/2} I_{3/2}(\eta_\tau) \quad (\text{A } 1)$$

Similarly, from Eqs. (12) and (19), the fragment density  $\rho_A$  comes out as

$$\rho_A = \frac{4\pi}{h^3} (2m_A^* T)^{3/2} J_{1/2}(\eta_A), \quad (\text{A.2})$$

or

$$\rho_A = \frac{2\pi}{h^3} (2m_A^* T)^{3/2} B_{1/2}(\eta_A), \quad (\text{A.3})$$

depending on whether the fragments are fermions or bosons. The  $J_k(\eta)$  and  $B_k(\eta)$  are the Fermi and Bose integrals,

$$\begin{aligned} J_k(\eta) &= \int_0^\infty \frac{x^k dx}{e^{(x-\eta)} + 1}, \\ B_k(\eta) &= \int_0^\infty \frac{x^k dx}{e^{(x-\eta)} - 1}. \end{aligned} \quad (\text{A.4})$$

The expression for  $V_\tau^0$  in Eq. (22) is given as,

$$\begin{aligned} V_\tau^0 &= -4\pi a^3 \{1 - d^2(2\rho_N)^\kappa\} (C_l \rho_\tau + C_u \rho_{-\tau}) \\ &+ \frac{16\pi^2 a^3}{b^2 h^3} \left[ C_l (2m_\tau^* T)^{5/2} J_{3/2}(\eta_\tau) + C_u (2m_{-\tau}^* T)^{5/2} \right. \\ &\times J_{3/2}(\eta_{-\tau}) \left. \right] + \frac{1}{2} I \rho_A \left\{ \left( \frac{\langle p_A^2 \rangle}{b^2} - 1 \right) (C_l \rho_{l\tau} + C_u \rho_{l-\tau}) \right. \\ &+ \frac{4\pi}{h^3 b^2} [C_l (2m_{l\tau}^{A*} T)^{5/2} J_{3/2}(\eta_{l\tau}^A) + C_u (2m_{l-\tau}^{A*} T)^{5/2} \\ &\times J_{3/2}(\eta_{l-\tau}^A)] + (C_l \rho_{l\tau} + C_u \rho_{l-\tau}) d^2 [\rho_N + \rho_l]^\kappa \left. \right\}. \end{aligned} \quad (\text{A.5})$$

In this equation, the fugacity  $\eta_{l\tau}^A$  is defined corresponding to the nucleons of density  $\rho_{l\tau}$  inside the fragment (exactly in parallel definition of the fugacity  $\eta_\tau$  of the free nucleons corresponding to the free nucleon density  $\rho_\tau$ );  $m_{l\tau}^{A*}$  is the effective mass of these nucleons.

Similarly, expressions for  $V_\tau^1, V_\tau^2, V_A^0$  and  $V_A^1$  are,

$$V_\tau^1 = \frac{4\pi a^3}{b^2} [C_l \rho_\tau + C_u \rho_{-\tau}] + \frac{1}{4} I (C_l + C_u) \frac{\rho_A \rho_l}{b^2}, \quad (\text{A.6})$$

$$\begin{aligned} V_\tau^2 &= 4\pi a^3 \kappa d^2 (2\rho_N)^{\kappa-1} \sum_{\tau'} [C_l \rho_{\tau'} + C_u \rho_{-\tau'}] \rho_{\tau'} \\ &+ \frac{1}{2} I \rho_A \rho_N (C_l \rho_{l\tau} + C_u \rho_{l-\tau}) \\ &\times [\kappa d^2 (\rho_N + \rho_l)^{\kappa-1}], \end{aligned} \quad (\text{A.7})$$

$$\begin{aligned} V_A^0 &= \frac{1}{2} I \sum_\tau \rho_\tau \left[ (C_l \rho_{l\tau} + C_u \rho_{l-\tau}) \left\{ -1 + \frac{4\pi (2m_\tau^* T)^{5/2}}{h^3 b^2 \rho_\tau} \right. \right. \\ &\times J_{3/2}(\eta_\tau) + d^2 \{ \rho_N + \rho_l \}^\kappa \left. \right\} \\ &+ \frac{4\pi}{b^2 h^3} \left\{ C_l (2m_{l\tau}^{A*} T)^{5/2} J_{3/2}(\eta_{l\tau}^A) \right. \\ &+ C_u (2m_{l-\tau}^{A*} T)^{5/2} J_{3/2}(\eta_{l-\tau}^A) \left. \right\} \\ &+ I_A \rho_A \sum_\tau \rho_{l\tau} \left\{ C_l \rho_{l\tau} \left( -1 + \frac{\langle p_A^2 \rangle}{b^2} + \frac{8\pi}{b^2 h^3} \right. \right. \\ &\times \frac{(2m_{l\tau}^{A*} T)^{5/2}}{\rho_{l\tau}} J_{3/2}(\eta_{l\tau}^A) \left. \right) + C_u \rho_{l-\tau} \left( -1 + \frac{\langle p_A^2 \rangle}{b^2} \right. \\ &+ \frac{4\pi (2m_{l\tau}^{A*} T)^{5/2}}{b^2 h^3} \frac{J_{3/2}(\eta_{l\tau}^A)}{\rho_{l\tau}} \\ &+ \frac{4\pi (2m_{l-\tau}^{A*} T)^{5/2}}{b^2 h^3} \frac{J_{3/2}(\eta_{l-\tau}^A)}{\rho_{l-\tau}} \left. \right\} \\ &+ I_A \rho_A d^2 \left[ \sum_\tau \rho_{l\tau} (C_l \rho_{l\tau} + C_u \rho_{l-\tau}) \right] (2\rho_l)^\kappa, \end{aligned} \quad (\text{A.8})$$

$$V_A^1 = \sum_\tau (C_l \rho_{l\tau} + C_u \rho_{l-\tau}) \left( \frac{I_A \rho_A}{b^2} \rho_{l\tau} + \frac{I}{2b^2} \rho_\tau \right). \quad (\text{A.9})$$

In Eqs. (A.5)-(A.8),  $\langle p_A^2 \rangle$  is the mean squared value of the fragment momentum in AN matter. Its value is given by,

$$\langle p_A^2 \rangle = (2m_A^* T) C_A, \quad (\text{A.10})$$

where  $C_A$  is given by Eqs. (40) or (41). The integrals  $I$  and  $I_A$  appearing in Eq. (A.5)-(A.9) for nucleon-nucleus and nucleus-nucleus interactions are given by,

$$I = \int_{V_A} d\mathbf{r} \int d\mathbf{R} \frac{e^{-|\mathbf{r}+\mathbf{R}|/a}}{|\mathbf{r}+\mathbf{R}|/a}, \quad (\text{A.11})$$

$$I_A = \int_{V_A} d\mathbf{r} \int_{V_A} d\mathbf{r}' \int d\mathbf{R} \frac{e^{-|\mathbf{R}+\mathbf{r}-\mathbf{r}'|/a}}{|\mathbf{R}+\mathbf{r}-\mathbf{r}'|/a}, \quad (\text{A.12})$$

Integrations on  $\mathbf{R}$  exclude the fragment volumes. The integrals are evaluated numerically.

[1] J. P. Bondorf, R. Donangelo, I. N. Mishustin, C. J. Pethick, H. Schultz, and K. Sneppen, Nucl. Phys. **A 443**, 321 (1985).

[2] J. P. Bondorf, A. S. Botvina, A. S. Iljinov, I. N. Mishustin, and K. Sneppen, Phys. Rep. **257**, 133 (1995).

[3] D. H. E. Gross, Rep. Prog. Phys. **53**, 605 (1990).

[4] Subrata Pal, S. K. Samaddar, A. Das, and I. N. De, Phys.

Lett. **B337**, 14 (1994).

[5] J. N. De, S. K. Samaddar, X. Vinas and M. Centelles, Phys. Lett. **B638**, 160 (2006).

[6] J. Pan and S. Das Gupta, Phys. Rev. C **51**, 1384 (1995).

[7] H. Müller and B. D. Serot, Phys. Rev. C **52**, 2072 (1995).

[8] T. Sil, S. K. Samaddar, J. N. De, and S. Shlomo, Phys. Rev. C **69**, 014602 (2004).

- [9] B. S. Meyers, *Annu. Rev. Astron. Astrophys.* **32**, 153 (1994).
- [10] C. J. Horowitz and A. Schwenk, *Nucl. Phys.* **A776**, 55 (2006).
- [11] J. N. De and S. K. Samaddar, *Phys. Rev. C* **78**, 065204 (2008).
- [12] G. Shen, C. J. Horowitz, and S. Teige, *Phys. Rev. C* **82**, 045802 (2010).
- [13] C. Ishizuka, A. Ohnishi, and K. Sumiyoshi, *Nucl. Phys.* **A723**, 517 (2003).
- [14] A. S. Botvina and I. N. Mishustin, *Phys. Lett.* **B584**, 233 (2004).
- [15] A. S. Botvina and I. N. Mishustin, *Nucl. Phys.* **A843**, 98 (2010).
- [16] M. Hempel and J. Schaffner-Bielich, *Nucl. Phys.* **A837**, 210 (2010).
- [17] S. Furusawa, S. Yamada, K. Sumiyoshi, and H. Suzuki, *Astrophys. J.* **738**, 178 (2011).
- [18] A. Le Fevre *et. al.*, *Phys. Rev. Lett.* **94**, 162701 (2005).
- [19] J. Iglio *et.al.*, *Phys. Rev. C* **74**, 024605 (2006).
- [20] D. V. Shetty, S. J. Yennello, and G. A. Souliotis, *Phys. Rev. C* **76**, 024606 (2007).
- [21] G. A. Souliotis, A. S. Botvina, D. V. Shetty, A. L. Keksis, M. Jandel, M. Veselsky, and S. J. Yennello, *Phys. Rev. C* **75**, 011601(R) (2007).
- [22] R. Ogul *et. al.*, *Phys. Rev. C* **83**, 024608 (2011); Erratum- *ibid.* **C 85**, 019903 (2012).
- [23] A. Ono, P. Danielewicz, W. A. Friedman, W. G. Lynch, and M. B. Tsang, *Phys. Rev. C* **68**, 051601 (2003).
- [24] S. K. Samaddar, J. N. De, X. Viñas, and M. Centelles, *Phys. Rev. C* **76**, 041602(R) (2007).
- [25] A. S. Botvina, N. Buyukcizmeci, M. Erdogan, J. Lukasik, I. N. Mishustin, R. Ogul, and W. Trautmann, *Phys. Rev. C* **74**, 044609 (2006).
- [26] N. Buyukcizmeci, A. S. Botvina, I. N. Mishustin, and R. Ogul, *Phys. Rev. C* **77**, 034608 (2008).
- [27] S. Typel, G. Röpke, T. Klähn, D. Blaschke, and H. H. Wolter, *Phys. Rev. C* **81**, 015803 (2010).
- [28] M. D. Voskresenskya and S. Typel, *Nucl. Phys.* **A887**, 42 (2012).
- [29] J. B. Natowitz *et.al.* , *Phys. Rev. Lett.* **104**, 202501 (2010).
- [30] K. Hagel *et.al.*, *Phys. Rev. Lett.* **108**, 062702 (2012).
- [31] W. D. Myers and W. J. Swiatecki, *Ann. Phys. (N.Y.)* **204**, 401 (1990).
- [32] J. N. De, N. Rudra, Subrata Pal, and S. K. Samaddar, *Phys. Rev. C* **53**, 780 (1996).
- [33] D. Bandyopadhyay, C. Samanta, S. K. Samaddar, and J. N. De, *Nucl. Phys.* **A511**, 1 (1990).
- [34] D. V. Shetty, S. J. Yennello, and G. A. Souliotis, *Phys. Rev. C* **75**, 034602 (2007).
- [35] P. Danielewicz, *Nucl. Phys.* **A727**, 233 (2003).
- [36] L. W. Chen, C. M. Ko, B. A. Li, and J. Xu, *Phys. Rev. C* **82**, 024321 (2010).
- [37] M. Warda, X. Viñas, X. Roca-Maza, and M. Centelles, *Phys. Rev. C* **80**, 024316 (2009).
- [38] X. Roca-Maza, M. Centelles, X. Viñas, and M. Warda, *Phys. Rev. Lett.* **106**, 252501 (2011).
- [39] L. W. Chen and J. Z. Gu, *J. Phys. G* **39**, 035104 (2012).
- [40] J. Dong, W. Zuo, J. Gu, and U. Lombardo, *Phys. Rev. C* **85**, 034308 (2012).
- [41] J. N. De and S. K. Samaddar, *Phys. Rev. C* **76**, 044607 (2007).
- [42] G. Shen, C. J. Horowitz, and S. Teige, *Phys. Rev. C* **83**, 035802 (2011).
- [43] S. K. Samaddar and J. N. De, *Phys. Rev. C* **83**, 055802 (2011).
- [44] D. G. Ravenhall, C. J. Pethick, and J. M. Lattimer, *Nucl. Phys.* **A407**, 571 (1983).
- [45] J. P. Blaizot, *Phys. Rep.* **64**, 171 (1980).
- [46] Jun Xu, Lie-Wen Chen, Bao-An Li, and Hong-Ru Ma, *Phys. Rev. C* **75**, 014607 (2007).
- [47] J. N. De and S. K. Samaddar, *Phys. Rev. C* **85**, 024310 (2012).
- [48] P. Bonche and D. Vautherin, *Nucl. Phys.* **A372**, 496 (1981).
- [49] J. M. Lattimer, C. J. Pethick, D. G. Ravenhall, and D. Q. Lamb, *Nucl. Phys.* **A432**, 646 (1985).
- [50] Toshiaki Maruyama, Toshitaka Tatsumi, Dmitri N. Voskresensky, Tomonori Tanigawa, and Satoshi Chiba, *Phys. Rev. C* **72**, 015802 (2003).
- [51] D. Bandyopadhyay, J. N. De, S. K. Samaddar, and D. Sperber, *Phys. Lett. B* **218**, 391 (1989).
- [52] S. Levit and P. Bonche, *Nucl. Phys.* **A437**, 426 (1985).
- [53] G. Auger *et.al.*, *Phys. Lett. B* **169**, 161 (1986).
- [54] E. Suraud, *Nucl. Phys.* **A462**, 109 (1987).